Identification of m6A-associated autophagy genes in non-alcoholic fatty liver

Ziqing Huang, Linfei Luo, Zhengqiang Wu, Zhihua Xiao and Zhili Wen

The Second Affiliated Hospital of Nanchang University, Nanchang, China

ABSTRACT

Background. Studies had shown that autophagy was closely related to nonalcoholic fat liver disease (NAFLD), while N6-methyladenosine (m6A) was involved in the regulation of autophagy. However, the mechanism of m6A related autophagy in NAFLD was unclear.

Methods. The NAFLD related datasets were gained *via* the Gene Expression Omnibus (GEO) database, and we also extracted 232 autophagy-related genes (ARGs) and 37 m6A. First, differentially expressed ARGs (DE-ARGs) and differentially expressed m6A (DE-m6A) were screened out by differential expression analysis. DE-ARGs associated with m6A were sifted out by Pearson correlation analysis, and the m6A-ARGs relationship pairs were acquired. Then, autophagic genes in m6A-ARGs pairs were analyzed for machine learning algorithms to obtain feature genes. Further, we validated the relationship between feature genes and NAFLD through quantitative real-time polymerase chain reaction (qRT-PCR), Western blot (WB). Finally, the immuno-infiltration analysis was implement, and we also constructed the TF-mRNA and drug-gene networks.

Results. There were 19 DE-ARGs and four DE-m6A between NAFLD and normal samples. The three m6A genes and five AGRs formed the m6A-ARGs relationship pairs. Afterwards, genes obtained from machine learning algorithms were intersected to yield three feature genes (TBK1, RAB1A, and GOPC), which showed significant positive correlation with astrocytes, macrophages, smooth muscle, and showed significant negative correlation with epithelial cells, and endothelial cells. Besides, qRT-PCR and WB indicate that TBK1, RAB1A and GOPC significantly upregulated in NAFLD. Ultimately, we found that the TF-mRNA network included FOXP1-GOPC, ATF1-RAB1A and other relationship pairs, and eight therapeutic agents such as R-406 and adavosertib were predicted based on the TBK1.

Conclusion. The study investigated the potential molecular mechanisms of m6A related autophagy feature genes (TBK1, RAB1A, and GOPC) in NAFLD through bioinformatic analyses and animal model validation. However, it is critical to note that these findings, although consequential, demonstrate correlations rather than cause-and-effect relationships. As such, more research is required to fully elucidate the underlying mechanisms and validate the clinical relevance of these feature genes.

Subjects Gastroenterology and Hepatology, Health Policy, Medical Genetics, Biomechanics

Keywords Non-alcoholic fatty liver disease, N6-methyladenosine, Autophagy, Immune infiltration analysis, Diagnosis

Submitted 23 October 2023
Accepted 5 February 2024
Published 29 February 2024

Corresponding author
Zhili Wen, wenzhili1@163.com

Academic editor
Vladimir Uversky

Additional Information and Declarations can be found on page 18

DOI **10.7717/peerj.17011**

How to cite this article Huang Z, Luo L, Wu Z, Xiao Z, Wen Z. 2024. Identification of m6A-associated autophagy genes in non-alcoholic fatty liver. *PeerJ* **12**:e17011 http://doi.org/10.7717/peerj.17011

INTRODUCTION

Non-alcoholic fatty liver disease (NAFLD) is a major cause of chronic liver disease, with a worldwide prevalence of approximately 25%. It is characterized by the accumulation of excessive triglycerides and other lipids in the hepatocytes (*Powell, Wong & Rinella, 2021*). NAFLD is a progressive disease that can progress from simple steatosis to steatohepatitis and eventually lead to cirrhosis or hepatocellular carcinoma (*Kanwal et al., 2018*). Owing to the current rapid changes in lifestyles, NAFLD is a public health issue and poses a great clinical and economic burden on the patient. Moreover, it has become the most prevalent liver disorder in China. China has been reported to have the fastest-growing prevalence of NAFLD in the world, with 314.58 million NAFLD individuals projected by 2030. It is also estimated that the population of NAFLD will increase from 80 million to 110 million in the USA by 2030 (*Estes et al., 2018*; *Zhou et al., 2020a*). However, the harmfulness and severity of NAFLD have not been paid enough attention. Currently, there are no standardised proposals by any country to address NAFLD at national and global levels (*Lazarus et al., 2022*).

NAFLD is a series of diseases involving excessive liver fat deposition, often accompanied by various metabolic disorders, there is a lack of specific therapeutic drugs (*Rong et al., 2022*). Non-pharmacological therapies that involve changes in diet and lifestyle are generally used, or indirect regulation and improvement of specific pathogenic factors, key links in the onset of the disease, and related metabolic disorders. For example, diosgenin (improving mitochondrial function), pomegranate (anti-inflammatory), curcumin (antioxidant) (*Chen et al., 2023*; *Zamanian et al., 2023*; *Beheshti Namdar et al., 2023*). The latest research shows that the interaction and regulation between serum metabolites and intestinal flora may help naringenin's therapeutic effect on NASH (*Cao et al., 2023*), and related studies targeting the intestinal-liver axis and regulating intestinal flora are constantly emerging (*Zhai et al., 2023*; *Wang et al., 2023*). On the other hand, another research evaluated disease-related circRNA and competitive endogenous RNA networks as potential biomarkers for NAFLD using functional gain and loss methods, reflecting the important role of targeted biomarker research in the progression of NAFLD (*Zeng et al., 2024*). Thus, we urgently need to elucidate the potential mechanisms of NAFLD.

Autophagy could maintains intracellular environmental homeostasis in response to external stimuli (*Hazari et al., 2020*), which is especially relevant to liver metabolism (*Byrnes et al., 2022*). Studies have shown that the dysregulation of autophagy is one of the important causes of NAFLD. Thus, the inhibition of autophagy can lead to an increase in the lipid droplet content of hepatocytes (*Cheng et al., 2019*). On the other hand, N6-methyladenosine (m6A) is the most pervasive internal modification of mRNA, which includes writers, erasers and readers (*He et al., 2019*). m6A affects the expression of target genes to maintain cellular functions and physiological processes by regulating mRNA processing, translation, degradation and splicing (*Liu & Gregory, 2019*; *Liu et al., 2017*). Currently, researchers have reported that the m6A modification plays an important role in the development of cancers and metabolic diseases (*Yang et al., 2019*; *Li et al., 2020*), and also in fatty liver disease (*Luo et al., 2019*). Importantly, it was reported that the autophagy

gene is closely associated with the m6A gene and fat mass and obesity (FTO), that the m6A demethylase can influence autophagy by decreasing the expression of ATG5 and ATG7 genes (*Wang et al., 2020*). Moreover, m6A writer methyltransferase like 3 (METTL3) and the m6A readers YTH N6-methyladenosine RNA binding protein 1 (YTHDF1) are negatively regulated autophagy pathway in NAFLD (*Peng et al., 2022*). Other studies also report that METTL3 regulates the m6A modification of lipid metabolism in hepatic cells and autophagy in cardiomyocytes (*Xie et al., 2019*). Considering the strong association between the m6A regulator and autophagy, we hypothesised that m6A-related autophagy genes may have important significance in NAFLD.

In this study, we aimed to screen the potential key m6A-related autophagy genes in NAFLD through comprehensive researches, and used bioinformatics tools to explore their potential function on NAFLD, including corresponding relationship with clinical features, immune features and transcription factor (TF) regulatory network. Further, the NAFLD animal model was built for the expression validation of key genes *in silico*. We make the case that the study could provide new biomarkers and a theoretical basis for the clinical diagnosis and treatment of NAFLD.

MATERIALS & METHODS

Data retrieved

The training set GSE66676 and validation set GSE130970 were downloaded *via* the Gene Expression Omnibus (GEO) (https://www.ncbi.nlm.nih.gov/gds) database, in which the GSE66676 contained 33 NAFLD samples and 34 normal samples (samples type: liver wedge biopsy) (*Xanthakos et al., 2015*), and GSE130970 validation set contained 72 NAFLD samples and three normal samples (samples type: liver biopsy) (*Hoang et al., 2019*). Additionally, 232 autophagy-related genes (ARGs) were extracted from the human autophagy database (HADb) (*Chen et al., 2022*) (http://www.autophagy.lu/), and 37 m6A were obtained from the literature (*Li et al., 2022*).

Differentially expressed ARGs and differentially expressed m6A genes were obtained using differential analysis

Based on the NAFLD and normal samples in the GSE66676 dataset, differentially expressed ARGs (DE-ARGs) and differentially expressed m6A genes (DE-m6A) were sifted out by limma package (v3.46.0) (*Wang et al., 2021*) setting $P < 0.05$. Meanwhile, volcano maps were plotted for the obtained results. Heat maps were drawn using the pheatmap package (v1.0.12) (*Zhang et al., 2021a*) to visualize the expression patterns of DE-ARGs and DE-m6A.

Construction of an m6A-ARGs co-expression network

Pearson correlation analysis was applied to analyse the relationships between DE-ARGs and DE-m6A using the cutoff Pearson correlation coefficient (PCC) >0.7 and $P < 0.05$, in which the gene selected were defined as the m6A-related autophagy genes (m6A-ARGs). The co-expression network of m6A-ARGs was drawn using the Cytoscape software. Then, WoLF-PSORT (https://wolfpsort.hgc.jp/) was used to predict the protein subcellular

localization (PSL) encoded by the m6A-ARGs. Finally, gene ontology (GO) and Kyoto Encyclopaedia of Genes And Genomes (KEGG) enrichment analysis of the m6A-ARGs were performed *via* the enrichGO and enrichKEGG functions in clusterprofiler R package (v3.18.1) for functionality annotations (*Yu et al., 2012*).

Screening and validation of feature genes

Support vector machine-recursive feature elimination (SVM-RFE) and random forest (RF) are increasingly used to predict disease-associated feature genes. We narrowed down the feature genes using SVM-RFE and RF on the m6A-ARGs using Caret R package (v6.0-92). The resultant genes obtained were intersected to obtain the feature genes. Further, we used the rank sum test setting the threshold $P < 0.05$ to evaluate the expression levels of the feature genes between NAFLD and normal samples in the GSE66676 and GSE130970 datasets, respectively. Finally, gene set enrichment analysis (GSEA) of the feature genes was performed setting the GO and KEGG as reference gene sets, where the correlation coefficient of the average expression of all genes in all samples and feature genes was calculated as the ranking standard, and then the gseGO (parameter settings: OrgDb = org.Hs.eg.db, ont = 'ALL', *p*valueCutoff = 0.05, *p*AdjustMethod = 'BH') and gseKEGG (parameter settings: organism = 'hsa', *p*valueCutoff = 0.05, pAdjustMethod = 'BH') functions in the clusterProfiler R package (v3.18.1) were conducted to perform GSEA analysis on the sorted genes. The entries that meet the conditions of |NES | >1, $P < 0.05$ and FDR <0.25 were considered to have significant meaning to be selected.

Correlation analysis of feature genes and clinicopathological characters

Based on the GSE66676 dataset, we analysed the correlation between feature genes and clinicopathological characters. The expression levels of the feature genes in different clinical states (borderline nonalcoholic steatohepatitis (NASH), definite NASH, NAFLD, not NASH, no NAFLD) were analysed using the Wilcoxon test. A box plot was drawn to visualize the results.

The mice model of NAFLD was constructed

Male C57/12 mice (12 weeks old) which were purchased from Guangdong Vital River Laboratory Animal Technology Co., Ltd. (Guangdong, China), were housed in animal care facilities with controlled temperature (21∼25 °C) and humidity (40∼70%), and light-dark cycles were 12 h. Twenty mice were randomly divided into normal group ($n = 10$) and NAFLD group ($n = 10$). The NAFLD group were fed 60% high fat diet (HFD), the other group with normal diet ,and the weight of these mice were monitored weekly, and their food intake were recorded accordingly. Mice do not suffer during the feeding process, after feeding for 12 weeks, they were euthanized painlessly (cervical dislocation under anesthesia 2% isoflurane), their liver tissue was taken out for examination. To ensure the successful establishment of a high-fat model, we conducted a pre-experiment before the formal experiment. The animal experiment was approved by the ethical review committee of The Second Affiliated Hospital of Nanchang University, the approval number: NCULAE-20221031008. All of the animal procedures in this study were in accordance with

the Laboratory animal-Guideline for ethical review of animal welfare promulgated by Standardization Administration of China and with the ARRIVE guidelines.

Hematoxylin-eosin staining

The liver sample was dealed according to the hematoxylin-eosin (HE) staining General processing procedure, Liver section morphological differences between normal and NAFLD groups in C57 mice were observed by HE staining.

Quantitative reverse transcriptase-PCR

qPCR verified the expression of RAB1A, TBK1, GOPC genes in two groups of male C57 mice. Using the Trizol method to extract the total RNA of liver tissue according to the manufacturer's instructions, the concentration of each RNA sample was detected. Then, the total RNA was converted to complementary deoxyribonucleic acid (cDNA) according to the the reverse transcription reagent kit. The quantitative PCR kit TB Green was used for cDNA for real-time PCR detection with the procedure: denaturation temperature 96 °C, annealing temperature 57 °C, extension temperature 72 °C for detection. Primers of qRT-PCR were listed in Table 1.

Western blotting detected the liver RAB1A, TBK1, GOPC protein content of C57 mice in the two group

The same weight of liver sample each group was taken and lysed with RIPA buffer to extracted the total proteins, which were quantified by using a microplate reader. Adding 1 μl of 5XSDS-PAGE protein loading buffer per 4 μL of protein sample before polyacrylamide gel electrophoresis, the subsequent routine western blot experimental steps are carried out, after the membranes were washed and successively incubated with the primary antibodies and the secondary antibody. The membrane was scanned on the Odyssey Li-COR CLx infrared laser scanner to obtain the content of RAB1A, TBK1, GOPC of rat liver.

Immune infiltration analysis

Body immunity plays an important role in the occurrence and development of diseases. Immune infiltration analysis was performed on the GSE66676 dataset, whereas xCell was used to observe the percentage distribution of immune cell types in each sample. Then, immune cells with differential distribution between NAFLD and normal samples were screened using the Wilcoxon test, and they were taken Spearman correlation analysis with feature genes by setting $P < 0.05$ and $|cor| > 0.3$. A scatter plot was drawn to visualize the results.

Construction of TF-mRNA network

TFs are a group of protein molecules that can be combined with specific sequences of genes to ensure that feature genes are expressed at a specific time and space. Differential TF-feature gene (TF-mRNA) relationship pairs were extracted from the hTFtarget database (https://ngdc.cncb.ac.cn/databasecommons/database/id/6946), and we also constructed a TF-mRNA regulatory relationship network according to the above relationship pairs.

Table 1 Primers of q-PCR.

	Forward primer	Reverse primer
Tbk1 (mouse)	TGTTCTAGAGGAGCCGTCCA	GGTGCACTATGCCGTTCTCT
Rab1a (**mouse**)	ATCGTTTCCCGTGGTTGGTT	ACACTGGTTGTGCTGTGTGA
GOPC (**mouse**)	CACTCTGTGGAGGATCTGGAAA	CTCGCCCCATAAACTTCAGC

Drug forecast analysis

To predict potential therapeutic drugs associated with feature genes, we uploaded the feature genes into the Drug-Gene Interaction database (DGIdb) (http://www.dgidb.org). Default parameters were used to analyse the interaction between drugs and feature genes. The results were visualized using Cytoscape.

Statistic analysis

Statistical analysis was carried out through R software. Differences between different groups were compared *via* the Wilcoxon test. $P < 0.05$ was considered as significant difference.

RESULTS

Identification of DE-ARGs and DE-m6A

The flowchart of data analysis is shown in Fig. 1. A total of 19 DE-ARGs was observed between NAFLD samples and normal samples, of which 15 were upregulated and four were downregulated DE-ARGs (Fig. 2A, Table 2). We also sifted out four DE-m6As (two up-regulated DE-m6As and two down-regulated DE-m6As) by differential expression analysis (Fig. 2B, Table 3).

m6A-ARGs co-expression network

Using the Pearson correlation analysis of DE-ARGs and DE-m6A (Fig. 3A), a total of three m6A genes, namely PCIF1, HNRNPA2B1 and SRSF10, and five ARGs, namely ATG4D, ATG5, TBK1, GOPC and RAB1A were obtained as the m6A-ARGs with PCC >0.7 and $P < 0.05$. The co-expression network visualized the interactions of PCIF1-ATG5, SRSF10-GOPC, HNRNPA2B1-ATG4D and other relationship pairs (Fig. 3B). Afterwards, the detected protein localization-distribution results in WoLF-PSORT analysis was displayed in Fig. 3C, in which the proteins encoded by TBK1 and ATG5 were presented in the cytoplasm, while those encoded by RAB1A and ATG4D were found in the extracellular matrix. Additionally, GOPC-encoded proteins were located in the nucleus. The enrichment analysis revealed that all genes in the m6A-ARGs co-expression network was involved in 10 GO pathways, such as macro-autophagy and selective autophagy (Fig. 3D). Autophagy can affect the development of NAFLD by reducing the degradation of intracellular lipid droplet closure and lysosomal fusion. Likewise, the results of KEGG analysis indicated that various m6A-ARGs were associated with the pathway of autophagy-animal, and the top10 enriched KEGG terms were showed in Fig. 3E.

Identification of feature genes

We respectively gained four and three genes *via* SVM-RFE and RF algorithms (Figs. 4A–4B), and they were intersected to yield three feature genes (TBK1, RAB1A and GOPC)

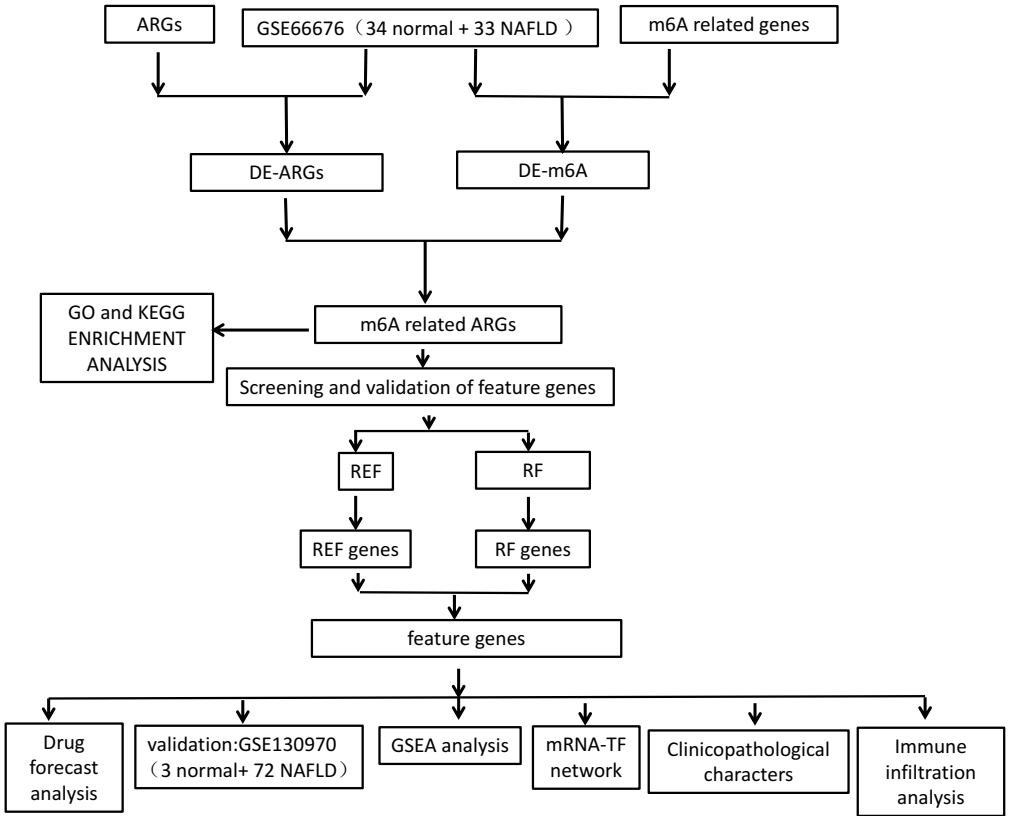

Figure 1 **Flowchart of overall study design.**

Full-size DOI: 10.7717/peerj.17011/fig-1

(Fig. 4C). According to the literature, TBK1 inhibitors alleviate the pathological response of NAFLD, suggesting that TBK1 is associated with NAFLD (*Oral et al., 2017*; *Huh et al., 2020*). Ras-related protein RAB1A is a member of the cellular G-protein Ras superfamily, which plays a role in protein transport and membrane remodeling. GOPC encodes a Golgi protein that had a PDZ structural domain, and Golgi proteins have been reported to play a role in intracellular protein transport and degradation. Nevertheless, the expression trends of three feature genes were the same in the GSE66676 (left) and GSE130970 (right) datasets, and they were significantly increased in NAFLD compared with normal samples (Fig. 4D).

The expression of feature genes are higher in rats with NAFLD ($n = 10$) than normal group ($n = 10$)

HE was used to verify the successful construct an *in vivo* model of NAFLD (Fig. 5A), the mRNA expression of TBK1, RABA1, GOPC were all significantly increased in the NAFLD group compared with the normal group (Fig. 5B). Meanwhile, the protein expression of TBK1, RABA1, GOPC were also increased in the NAFLD group than the normal group (Figs. 5C–5D), the result showed that the three feature genes may play an important role in NAFLD.

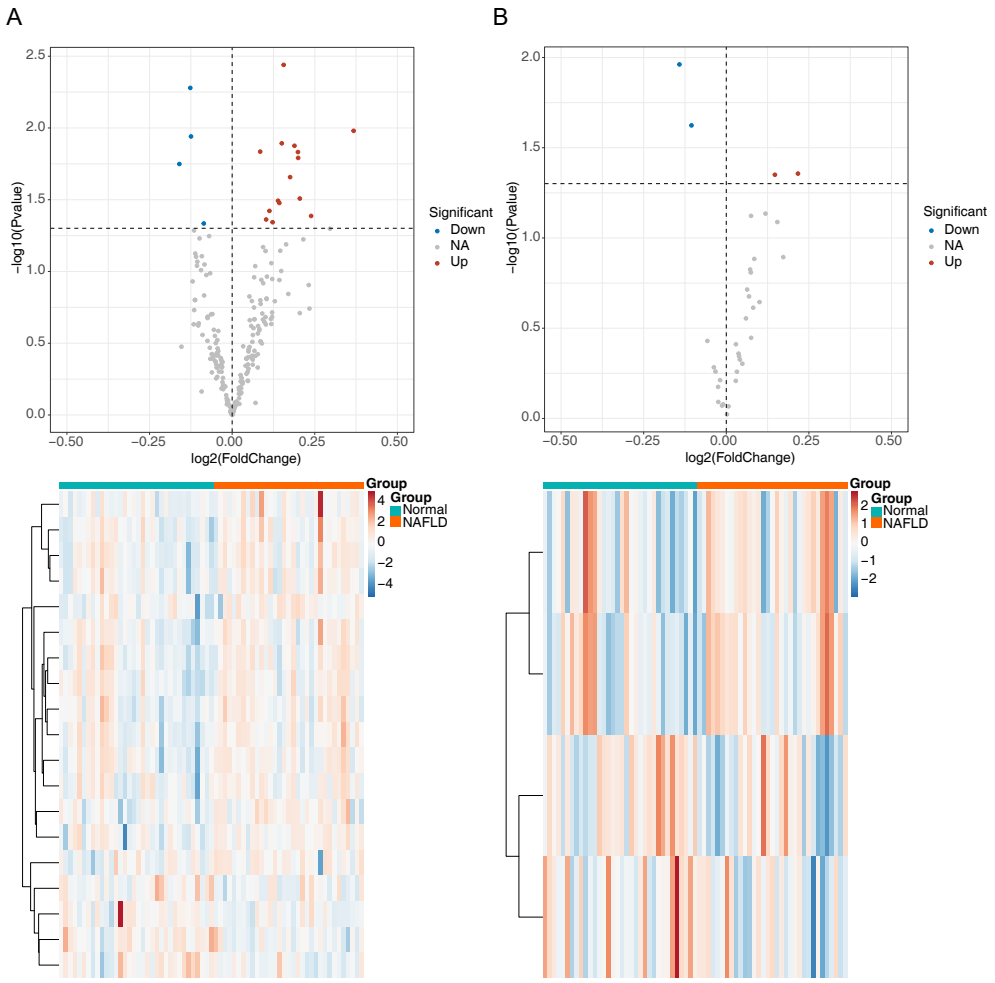

Figure 2 Identification of differentially expressed autophagy related genes (DE-ARGs) and differentially expressed m6A genes (DE-m6A). (A) Volcano plot (top) and heat map (bottom) of DE-ARGs between NAFLD and normal samples in GSE66676, red represents up-regulation, blue represents down-regulation. (B) Volcano plot (top) and heat map (bottom) of DE-M6A genes in GSE66676. For A–B, $P < 0.05$ was set as significant differences. The rows in the heat map represent the expression patterns of each gene in samples from different sources (green: Normal; orange: NAFLD), and the columns represent the expression patterns of different genes in each sample (blue: downregulation; red: upregulation), where the cluster tree on the left represents the genes with similar expression patterns were clustered.

Full-size DOI: 10.7717/peerj.17011/fig-2

Enrichment and clinical correlation analyses of feature genes

TBK1 was enriched in 1,861 GO pathways, such as the catalytic step 2 spliceosome, and it was enriched to 150 KEGG pathways, including fatty acid degradation, protein export and so on (Fig. 6A). RAB1A was enriched in 1,408 GO pathways, including antigen processing and presentation of peptide antigen *via* MHC class I, and 108 KEGG pathways, including the proteasome pathway (Fig. 6B). A total of 2,068 GO pathways were enriched by GOPC, including the ribonucleoprotein complex biogenesis, and 149 KEGG pathways were obtained, including nucleocytoplasmic transport (Fig. 6C). Furthermore, the box

Table 2 Lists for the differentially expressed autophagy related genes (DE-ARGs) between NAFLD and normal samples in GSE66676.

	logFC	AveExpr	*t*	*P*.value	adj. *P*.val	B
CDKN1B	0.155991255	7.791996413	3.009818825	0.00363408	0.381531286	−2.054356556
ATG4D	−0.126722986	6.893206907	−2.881078481	0.005258718	0.381531286	−2.309982934
HSPA5	0.367701476	10.80340176	2.63104235	0.010464713	0.381531286	−2.782569957
ITGB4	−0.12442223	5.509958325	−2.596851071	0.011461408	0.381531286	−2.844637478
GOPC	0.150314626	7.564719096	2.55511884	0.012794154	0.381531286	−2.919533697
EIF2AK3	0.188627977	6.914901924	2.540104874	0.013306904	0.381531286	−2.946245686
IKBKB	0.084903034	7.375056448	2.503880459	0.01462123	0.381531286	−3.010181302
RHEB	0.199168958	7.335165	2.501335584	0.01471782	0.381531286	−3.014645578
HSP90AB1	0.199743343	10.09404822	2.46475225	0.016171234	0.381531286	−3.078420713
PPP1R15A	−0.159745345	6.108658464	−2.426477422	0.017828565	0.381531286	−3.144337995
TBK1	0.175433344	7.21801386	2.342607025	0.02200197	0.42803833	−3.285855566
RAB1A	0.204874846	9.768151338	2.201047573	0.031037081	0.509247311	−3.515394688
WIPI1	0.138979281	7.753411242	2.186279158	0.032145563	0.509247311	−3.538653978
MAPK9	0.142781973	7.815001148	2.171171147	0.033315245	0.509247311	−3.562311787
HDAC6	0.112872637	8.079616328	2.116973775	0.037822661	0.5215983	−3.646038191
DNAJB9	0.239011167	7.756817388	2.081609315	0.041041743	0.5215983	−3.699700039
BECN1	0.102938592	7.101400105	2.056883887	0.043430886	0.5215983	−3.736758985
ATG5	0.122487529	7.607437523	2.037567537	0.045379987	0.5215983	−3.765446156
IFNG	−0.085846797	3.768942053	−2.028600253	0.046310129	0.5215983	−3.778684503

Table 3 Lists for the differentially expressed m6A (DE-m6A) genes between NAFLD and normal samples in GSE66676.

	logFC	AveExpr	*t*	*P*.value	adj. *P*.val	B
CDKN1B	0.155991255	7.791996413	3.009818825	0.00363408	0.381531286	−2.054356556
ATG4D	−0.126722986	6.893206907	−2.881078481	0.005258718	0.381531286	−2.309982934
HSPA5	0.367701476	10.80340176	2.63104235	0.010464713	0.381531286	−2.782569957
ITGB4	−0.12442223	5.509958325	−2.596851071	0.011461408	0.381531286	−2.844637478
GOPC	0.150314626	7.564719096	2.55511884	0.012794154	0.381531286	−2.919533697
EIF2AK3	0.188627977	6.914901924	2.540104874	0.013306904	0.381531286	−2.946245686
IKBKB	0.084903034	7.375056448	2.503880459	0.01462123	0.381531286	−3.010181302
RHEB	0.199168958	7.335165	2.501335584	0.01471782	0.381531286	−3.014645578
HSP90AB1	0.199743343	10.09404822	2.46475225	0.016171234	0.381531286	−3.078420713
PPP1R15A	−0.159745345	6.108658464	−2.426477422	0.017828565	0.381531286	−3.144337995
TBK1	0.175433344	7.21801386	2.342607025	0.02200197	0.42803833	−3.285855566
RAB1A	0.204874846	9.768151338	2.201047573	0.031037081	0.509247311	−3.515394688
WIPI1	0.138979281	7.753411242	2.186279158	0.032145563	0.509247311	−3.538653978
MAPK9	0.142781973	7.815001148	2.171171147	0.033315245	0.509247311	−3.562311787
HDAC6	0.112872637	8.079616328	2.116973775	0.037822661	0.5215983	−3.646038191
DNAJB9	0.239011167	7.756817388	2.081609315	0.041041743	0.5215983	−3.699700039
BECN1	0.102938592	7.101400105	2.056883887	0.043430886	0.5215983	−3.736758985
ATG5	0.122487529	7.607437523	2.037567537	0.045379987	0.5215983	−3.765446156
IFNG	−0.085846797	3.768942053	−2.028600253	0.046310129	0.5215983	−3.778684503

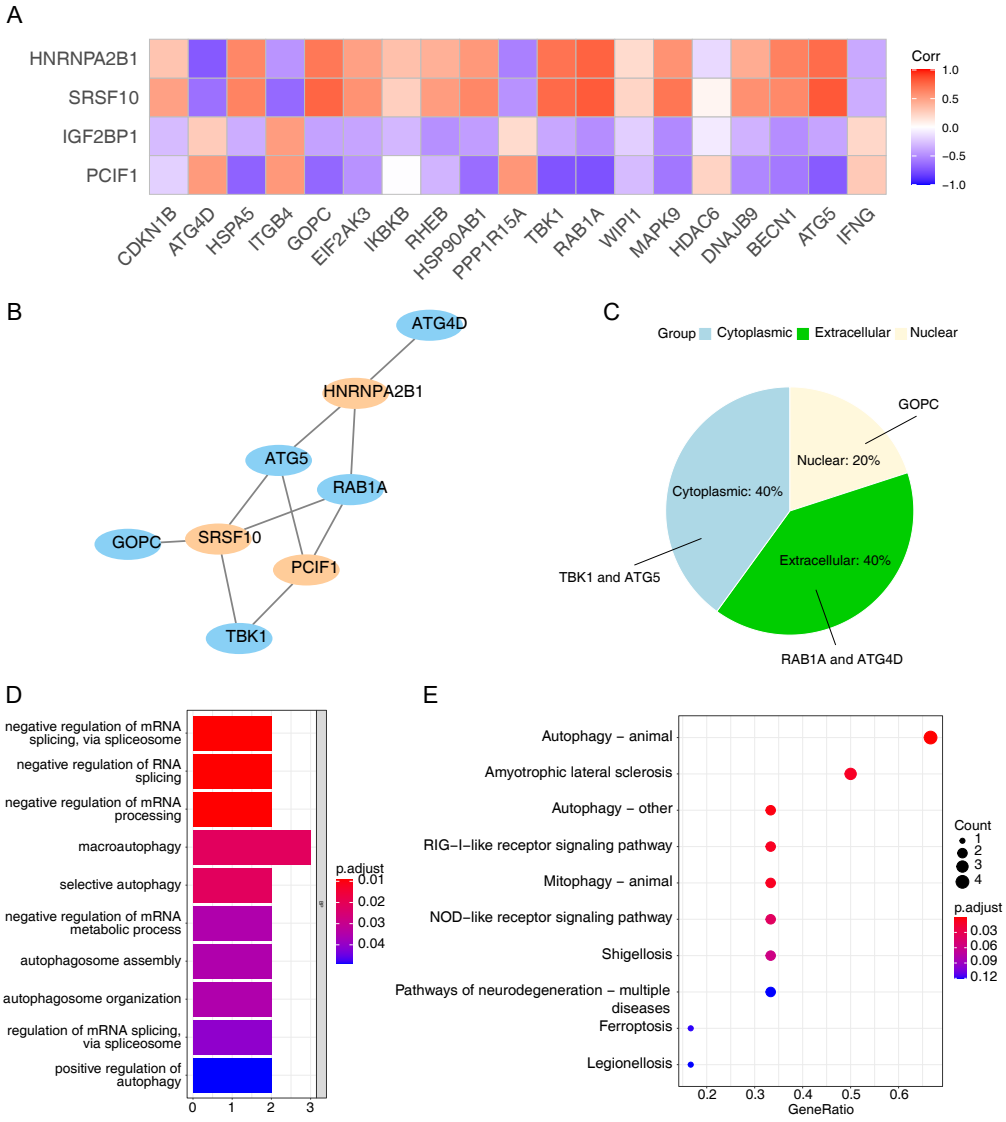

Figure 3 **Collection of m6A-related autophagy genes (m6A-ARGs).** (A) Pearson correlation heatmap of DE-ARGs and DE-m6A to screen m6A-ARGs using the cutoff pearson correlation coefficient (PCC) > 0.7 and $P < 0.05$. The abscissa is the DE-ARGs, the ordinate is DE-m6A. (B) Visualization of the co-expression network among m6A-ARGs *via* Cytoscape. Blue represents ARG and orange represents m6A gene. (C) Pie chart of WoLF-PSORT results for the predicted protein subcellular localization (PSL) which was encoded by m6A-ARGs. (D–E) Gene Ontology (GO) and Kyoto Encyclopaedia of Genes and Genomes (KEGG) enrichment analysis of all genes in the m6A-ARGs co-expression network.

Full-size DOI: 10.7717/peerj.17011/fig-3

plot revealed that the expressions of TBK1, RAB1A and GOPC in borderline NASH, define NASH, NAFLD, not NASH and no NAFLD were significantly different (Fig. 6D).

Immune micro environment analysis

The percentage distribution of eight immune cells, such as astrocytes, chondrocytes, and epithelial cells, were all dramatically different between NAFLD and normal samples

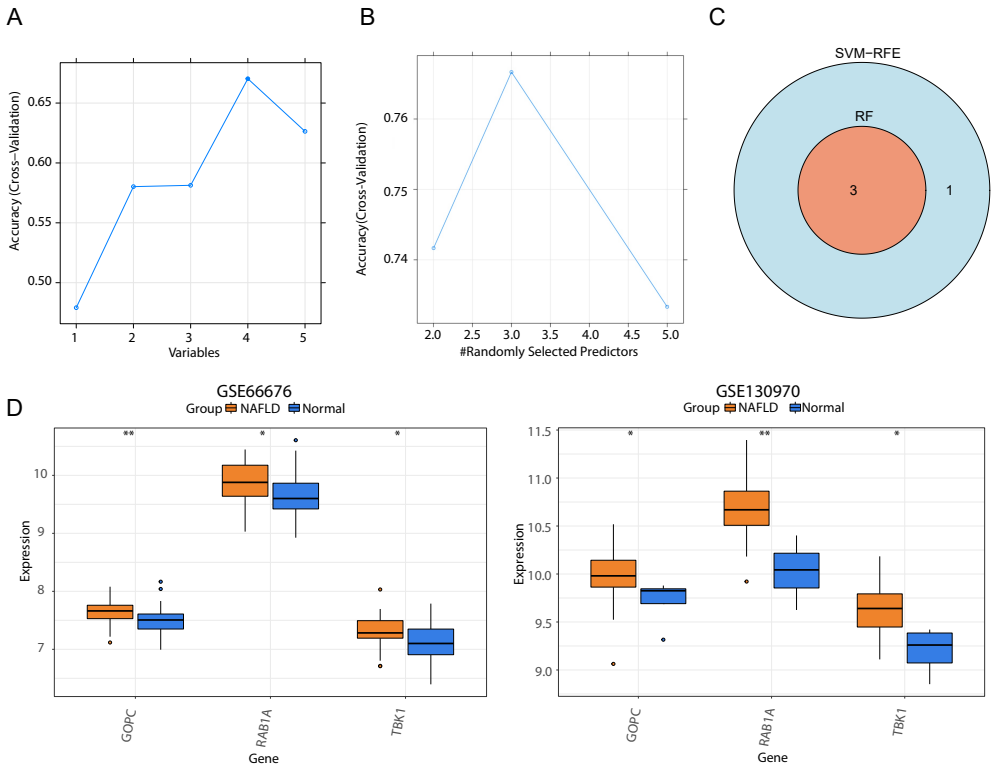

Figure 4 Screening of three feature genes and expression verification in two public datasets. (A) Four candidate genes were selected in the support vector machine-recursive feature elimination (SVM-RFE) model. The abscissa indicates the number of feature genes in RFE analysis, the ordinate represents the accuracy of the model. Blue line refers to the tendency of accuracy with the number of feature genes. (B) Three candidate genes were selected by the random forest (RF) model. (C) Venn diagram for three feature genes shared by two models. (D) Box plots of the expression levels of three feature genes between normal and disease samples in GSE66676 (left) and GSE130970 (right). $^{**}p < 0.01$, $^{*}p < 0.05$.

Full-size DOI: 10.7717/peerj.17011/fig-4

(Fig. 7A). Correlation analysis revealed that RAB1A, TBK1 and GOPC were significantly positively correlated with astrocytes, macrophages and smooth muscle but negatively correlated with epithelial cells and endothelial cells (Figs. 7B–7G).

TF-mRNA regulatory relationship network

The GOPC, RAB1A and TBK1 was related to 37, 33 and 54 TF-mRNA pairs, respectively, and the TF-mRNA network included FOXP1-GOPC, ATF1-RAB1A, AR-TBK1 and other relationship pairs (Fig. 8).

Drug sensitivity analysis

For the predicted therapeutic agents from the DGIdb database, data on GOPC and RAB1A was absence. Based on TBK1, we finally predicted eight therapeutic agents, namely R-406, adavosertib, chembl-1997335, PF-00562271, CYC-116, TAE-684, cenisertib and entrectinib (Fig. 9).

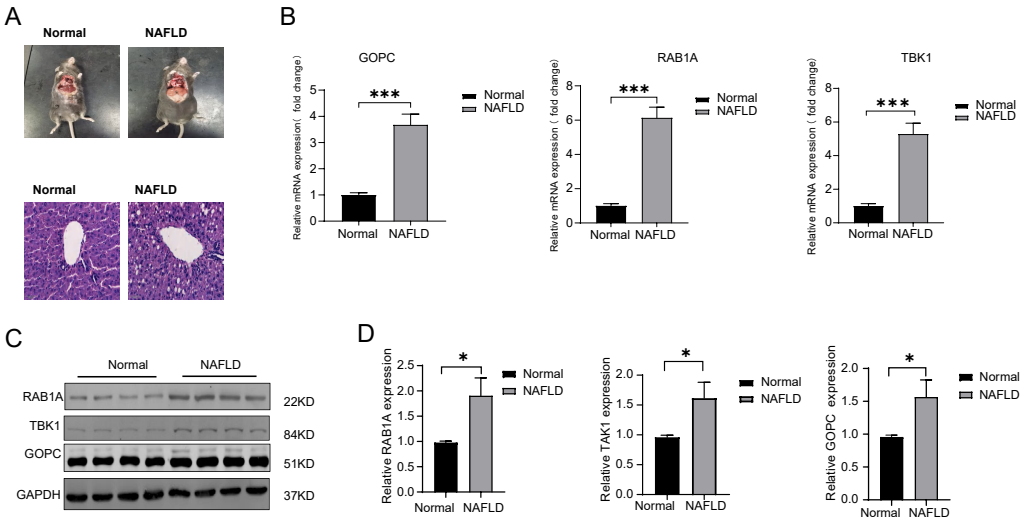

Figure 5 The mRNA and protein expression of TBK1, RAB1A and GOPC in animal model. (A) Hematoxylin-eosin (HE) staining image as the pathological evidence for treatment of NAFLD. (B) Quantitative reverse transcriptase-PCR (qRT-PCR) showed the mRNA expression of the three feature genes were significantly higher in NAFLD rats ($n = 10$) than in normal rats ($n = 10$). (C–D) Western blotting (WB) showed that the three feature genes was significantly higher in NAFLD rats ($n = 5$) than in normal rats ($n = 5$). * $P < 0.05$, *** $P < 0.001$.

Full-size DOI: 10.7717/peerj.17011/fig-5

DISCUSSION

M6A RNA methylation regulators play a role in preventing age-related and diet-induced development of NAFLD by improving inflammatory and metabolic phenotypes (*Peng et al., 2022*; *Qin et al., 2021*). However, knowledge of the biological role of m6A-related autophagy genes in the development of NAFLD is lacking. Recently research has shown autophagy is associated with the development of NAFLD, four autophagy-related lncRNAs were be found may participate in the occurrence of NAFLD (*Cao et al., 2022*). In this study, we explored differentially expressed m6A genes and autophagy genes in NAFLD and constructed an m6A-autophagy genes co-expression network using machine learning algorithms (SVM-RFE and RF) to filter out signature genes (*Chen & Ishwaran, 2012*; *Sanz et al., 2018*). Three feature genes, namely TBK1, RAB1A and GOPC were selected as the biomarkers of NAFLD.

TANK Binding Kinase 1 (TBK1), a protein-coding gene, is a critical kinase that modulates inflammation and autophagy. It was reported that the abnormal expression of TBK1 is related to obesity, diabetes, even and NAFLD (*He et al., 2020*; *Xu et al., 2018*). That is, as a member of the non-canonical IKK family, TBK1 is considered a by-product of activating the NF- κB signalling pathway in the liver (*Zhao et al., 2018*). Blocking the IKK ε and TBK1 pathways can significantly reduce the inflammatory factors produced by pro-inflammatory cells such as TNF- α and MCP-1, thereby improving insulin sensitivity and reducing liver steatosis (*Reilly et al., 2013*). TBK1 can reduce the thermogenesis and catabolism of the mitochondria by inhibiting the activity of AMPK, resulting in energy storage and ultimately

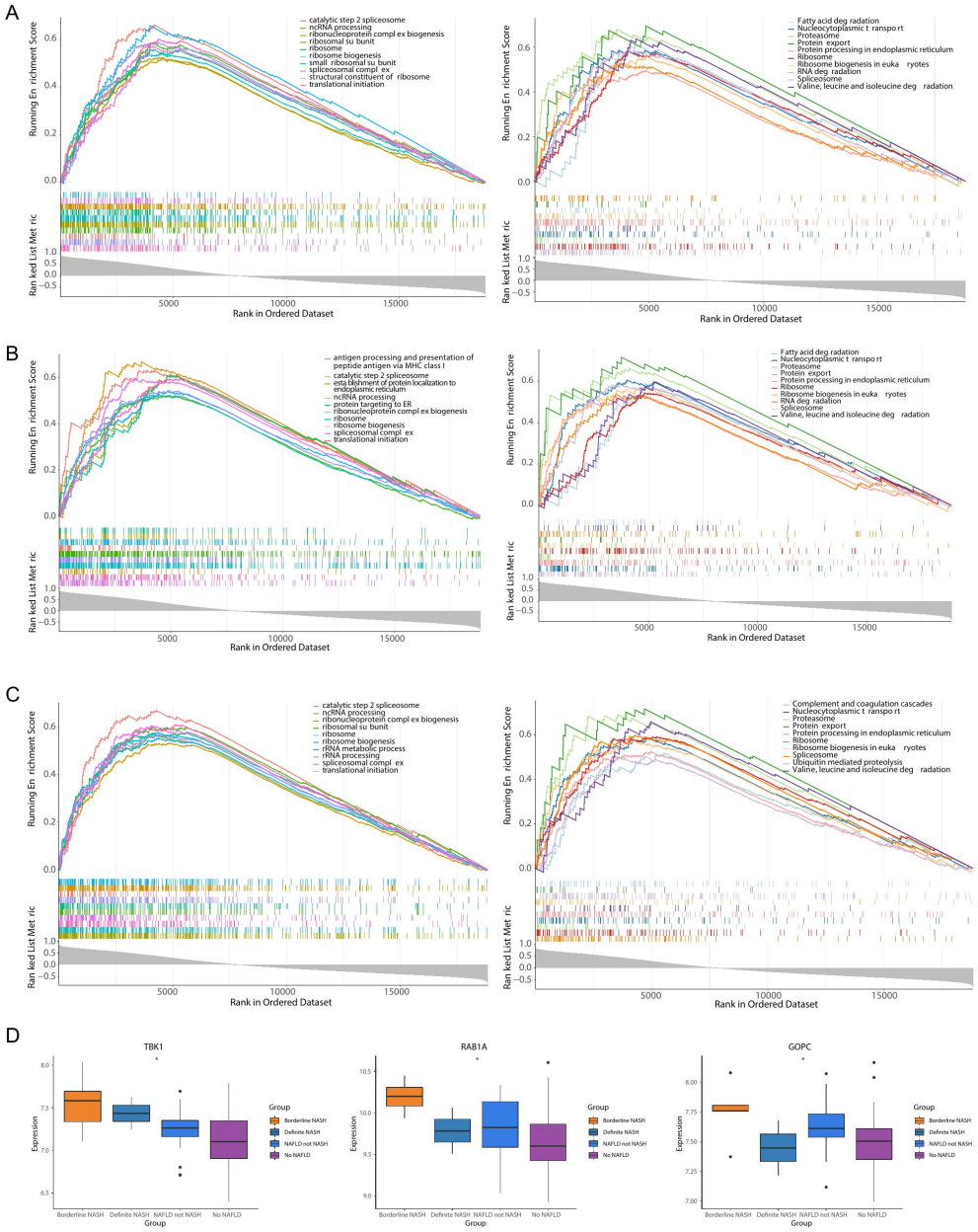

Figure 6 Functionality and correlations with clinicopathological characters of three feature genes in the GSE66676 dataset. (A–C) Gene set enrichment analysis (GSEA) of three feature genes (left: GO; right: KEGG). (A) *TBK1*. (B) *RAB1A*. (C) *GOPC*. Each figure shows partial enrichment entries (top 10). The figure contains three parts. The top of the figure refer to the enrichment score (ES) of each gene. A particularly obvious peak on the left is the ES value on the phenotype of the gene set. Each line in the middle of the figure represents a gene in the gene set and its ranking position in the gene list. The bottom of the figure shows a matrix of gene-phenotype correlations. (D) Box plots of the expression of *TBK1*, *RAB1A*, *GOPC* in different clinical states (borderline nonalcoholic steatohepatitis (NASH), definite NASH, NAFLD, not NASH, and no NAFLD. $^{***}p < 0.001$, $^{**}p < 0.01$, $^{*}p < 0.05$).

Full-size DOI: 10.7717/peerj.17011/fig-6

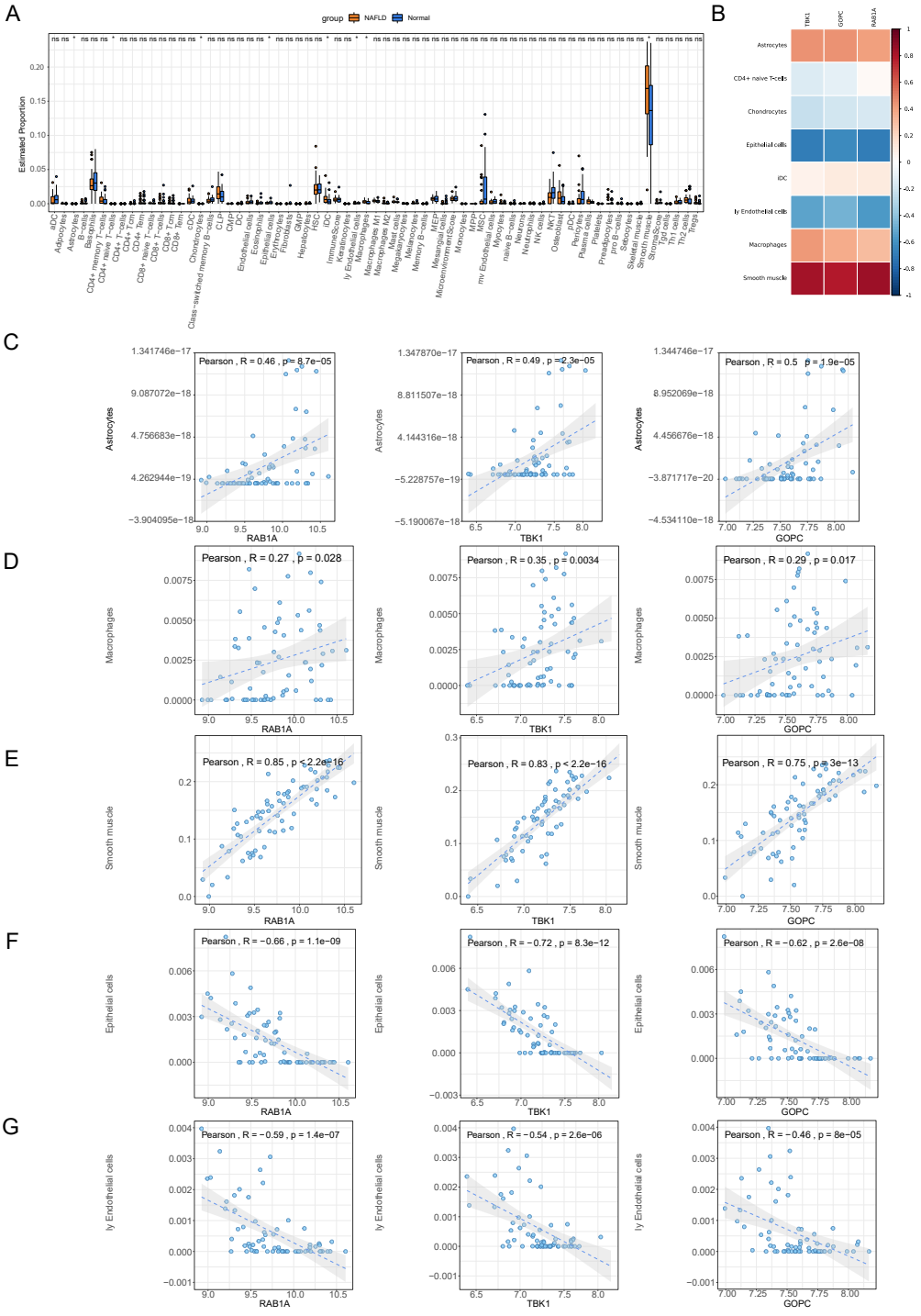

Figure 7 **Immune correlation analysis.** (A) Box plot for the proportions of immune cells subtypes in NAFLD and normal samples from the GSE66676 dataset (xCell algorithm). (B) Correlation heat map of eight differential expressed immune cells with feature genes. (C–G) Scatter plot for correlations of five significant immune cells with feature genes. (C) Astrocytes. (D) Macrophages. (E) Smooth muscle. (F) Epithelial cells. (G) Endothelial cells.

Full-size DOI: 10.7717/peerj.17011/fig-7

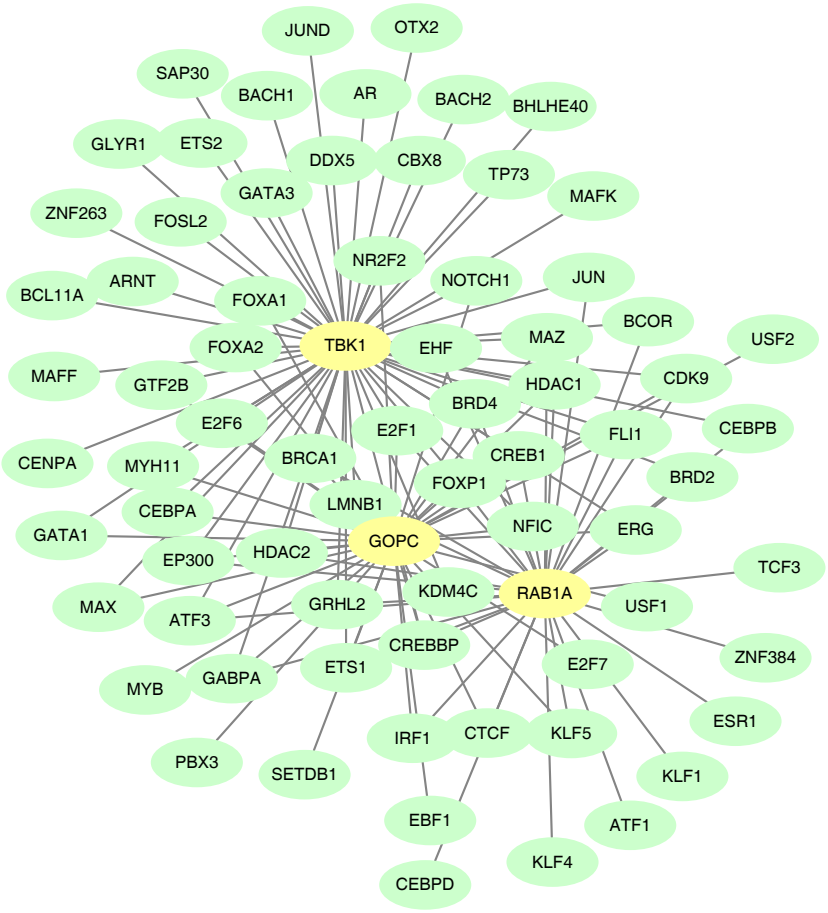

Figure 8 **Construction of the transcription factor (TF)-mRNA regulatory network.** Green is TF and yellow is feature gene.

Full-size DOI: 10.7717/peerj.17011/fig-8

leading to obesity (*Zhao et al., 2018*). It has been reported that TBK1 is increased in palmitic acid (PA)-treated liver cells (especially in liver Kupffer cells), suggesting its potential role in the progression of NAFLD to NASH. Corresponding to it, TBK1 inhibitors can alleviate PA-mediated lipid accumulation, inflammatory reaction and adipocyte apoptosis in hepatocytes (*Zhou et al., 2020b*), indicating the vital indicative significance of TBK1 in the progression of NAFLD.

RAB1A is notable for its role in vesicular trafficking and is generally considered to be a housekeeping protein that regulates cell membrane dynamics (*Yang et al., 2016*). The abnormal expression of RAB1A has been associated with many human diseases, such as glucose homeostasis, Parkinson's disease and various cancers (*Zhang et al., 2021b*; *Coune et al., 2011*; *Huang et al., 2021*). Autophagy generally provides a protective function by limiting tumour necrosis and inflammation, thereby reducing the damage of tumour cells to the body. Studies have shown that the overexpression of RAB1A in cancer cells may promote autophagy progression by effecting with optic nerve protein (OPTN, an autophagy

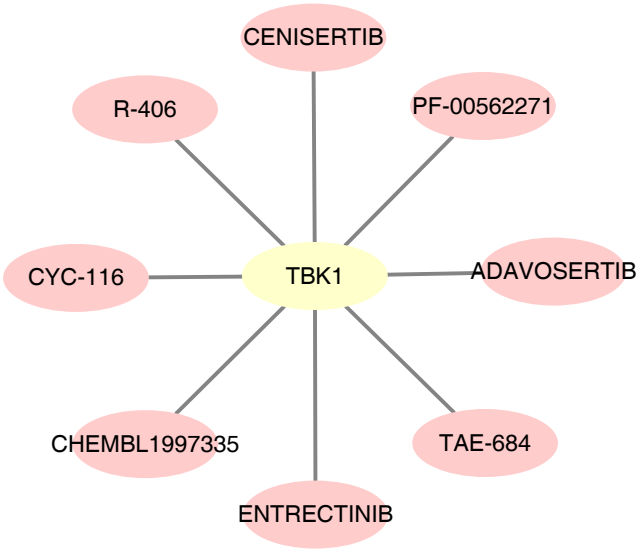

Figure 9 **Potential drugs targeting feature genes.** Yellow represents gene and pink represents drug.
Full-size DOI: 10.7717/peerj.17011/fig-9

receptor). The knockout of RAB1A not only prevents endoplasmic reticulum-Golgi transport but also inhibits autophagy formation (*Song et al., 2018*). Meanwhile, RAB1A interacts with C9orf72 to regulate the initiation of autophagy by regulating the transport of the ULK1 autophagy initiation complex to phagocytic cells (*Webster et al., 2016*). A recent study reported that RAB1A plays a role in autophagy by recruiting and directly activating autophagy-specific VPS34 complex I (VPS34/VPS15/Beclin 1/ATG14L) (*Tremel et al., 2021*). However, most existing studies on RAB1A are regarding its role in tumours, with hardly any studies on its role in NAFLD. In this study, the samples in NAFLD groups had a up-regulated levels of RAB1A, which might be used as a reference for future studies on its role in NAFLD.

GOPC plays a role in intracellular protein trafficking and degradation. It also regulates the intracellular trafficking of the ADR1B receptor and plays a role in autophagy (*He et al., 2004*; *Cheng et al., 2002*). In this study, the abnormal up-regulation of GOPC expression was observed in NAFLD, while, very few studies on GOPC exist, thus, we need more experiments to explore its function in NAFLD. In our study, the TBK1, RABA1,GOPC were confirmed higher expressed in NAFLD through rats models and *in silico*. Previous studies have confirmed the importance of TBK1 in the development of NAFLD. Some related pharmacological treatments refer to TBK1 in NAFLD have also been reported. Although there are no studies research about RABA1 and GOPC in NAFLD, but we still thought RABA1 and GOPC may be plays important role in the occurrence of NAFLD. This study provides some theoretical basis for in-depth research between RABA1 and GOCP with NAFLD.

Currently, the pathogenesis of NAFLD is yet to be wholly elucidated. The pathogenesis of NAFLD involves a variety of factors, such as environmental factors, obesity, changes

in microbiota and susceptibility to gene mutations, among which imbalance of pro-inflammatory and anti-inflammatory cytokines within adipose tissue plays a key role in the pathological process of NAFLD (*Arab, Arrese & Trauner, 2018*; *Paredes-Turrubiarte et al., 2016*). In the study, immune infiltration analysis demonstrated that the different proportions of astrocytes, naïve CD4+ T cells, chondrocytes, epithelial cells, iDC, endothelial cells, macrophages and smooth muscle might be involved in NAFLD's pathogenesis. Macrophage is an important component of liver inflammation, with activated macrophages secreting various pro-inflammatory cytokines, such as TNF- α, TGF- β1 and IL-6 (*Paredes-Turrubiarte et al., 2016*; *Kakino et al., 2018*). Notably, a recent study demonstrated that macrophages can induce hepatic TBK1 activation and expression (*Zheng et al., 2021*), which is consistent with our findings. Our study revealed that TBK-1, RAB-1A and GOPC were positively correlated with macrophages. Additionally, M2 Kupffer cells can promote the apoptosis of M1 Kupffer cells by secreting IL-10, consequently inhibiting the development of NASH (*Wan et al., 2014*). Dendritic cells can reduce the inflammatory reaction of NASH by clearing necrotic fragments and apoptotic bodies in the liver (*Henning et al., 2013*). The current study demonstrated a negative correlation between iDCs and the expression of TBK-1, RAB-1A and GOPC. The number of NKT cells is reduced in the presence of moderate to severe fatty inflammation, and the upregulation of NKT cells in the liver can relieve the hepatic steatosis induced by a high-fat diet. When NKT cells are over-depleted, the metabolic changes subsequently lead to NASH progression (*Tang et al., 2022*). In our study, TBK1, RAB1A and GOPC also showed a significant positive correlation with the expression of astrocytes and smooth muscle. The study of a single inflammatory factor and its interaction mechanism in NAFLD will aid in elucidating its pathogenesis in NAFLD. Currently, pro-inflammatory factor-related inhibitors have entered the clinical trial stage and are expected to become specific drugs for the treatment of NAFLD.

TFs are specific sites in the promoter sequence of target genes that regulate the expression level of downstream genes on a pre-transcriptional level by binding to the specific sequence motif (*Zacksenhaus et al., 2017*; *Zhang, Najmi & Schneider, 2017*). A large number of related studies have reported that TFs play an important role in the transcriptional regulatory network. Approximately 32 TFs can regulate ARGs to control autophagy in NAFLD (*Ueno & Komatsu, 2017*; *Di Malta, Cinque & Settembre, 2019*). Notably, cAMP response element-binding protein (CREB) and forkhead box O proteins are the most representative TFs and can upregulate autophagy genes and influence glucose and lipid metabolism (*Seok et al., 2014*; *Xiong et al., 2012*). In our study, 124 TF-mRNAs pairs of feature genes were identified, among which CREB-1 was associated with the three feature genes. Notably, CREB-1 has been reported to alleviate NAFLD *via* the CREB pathway (*Xu et al., 2022*).

The therapeutic agents which target TFs could prevent the progression of NAFLD into NASH. This study predicted eight therapeutic agents, which are based on TBK1, for the treatment of NAFLD. R-406 is a spleen tyrosine kinase inhibitor that can inhibit the SKY signalling pathway induced by LPS- and IFN- γ in macrophages. R-406 is also upregulated in hepatocytes (*Qu et al., 2018*). Moreover, it reduces immune complex-mediated inflammation through dose-dependently inhibited nitric-oxide release and

M1-specific markers in M1-differentiated macrophage. It can also significantly relieve liver inflammation, which could be a potential therapeutic approach for the treatment of NASH (*Kurniawan et al., 2018*). However, studies on the other seven therapeutic agents identified herein are scarce, remains to be further examined.

This study has certain shortcomings. Firstly, the sample size of the training set is small, which requiring subsequent larger cohorts to verify the expression and diagnostic performance of three feature genes. Secondly, further functional experiments *in vivo* and *in vitro* targeting the feature genes are required for exploring the causality as well as exact effect of the identified genes on the pathogenesis of NAFLD. Thirdly, the connections as well as underlying regulatory mechanism of predicted TFs binding sites and m6A-related autophagy genes are necessary to examine through more studies.

CONCLUSIONS

In conclusion, three m6A-related autophagy genes, namely TBK1, RAB1A and GOPC, were considered to be relevant to NAFLD progression based on various bioinformatic analyses. Differences of the expression levels of key genes between case and control samples were examined through two online NAFLD-related cohorts and animal models. The strong correlations of three key with smooth muscle, endothelial cells were explored as well. The potential TF binding sites and drugs targeting three genes were predicted, which initially provides a systematically comprehensive analysis of m6A-related autophagy genes in NAFLD and predicts potential agents for the treatment of NAFLD. Nonetheless, further exploration of m6A-related autophagy genes would aid in elucidating the mechanism of occurrence in NAFLD, thereby improving NAFLD treatment options.

ACKNOWLEDGEMENTS

We would like to thank all the reviewers who participated in the review and BULLET Editor for its linguistic assistance during the preparation of this manuscript.

ADDITIONAL INFORMATION AND DECLARATIONS

Funding

This work was supported by the National Natural Science Foundation of China (grant number 81960440 and grant number 82070594). The funders had no role in study design, data collection and analysis, decision to publish, or preparation of the manuscript.

Grant Disclosures

The following grant information was disclosed by the authors:
National Natural Science Foundation of China: 81960440, 82070594.

Competing Interests

The authors declare there are no competing interests.

Author Contributions

- Ziqing Huang conceived and designed the experiments, analyzed the data, prepared figures and/or tables, and approved the final draft.
- Linfei Luo performed the experiments, prepared figures and/or tables, and approved the final draft.
- Zhengqiang Wu performed the experiments, prepared figures and/or tables, and approved the final draft.
- Zhihua Xiao analyzed the data, authored or reviewed drafts of the article, and approved the final draft.
- Zhili Wen conceived and designed the experiments, analyzed the data, authored or reviewed drafts of the article, and approved the final draft.

Animal Ethics

The following information was supplied relating to ethical approvals (*i.e.*, approving body and any reference numbers):

The animal experiment was approved by the ethical review committee of The Second Affiliated Hospital of Nanchang University (approval number: NCULAE-20221031008).

Data Availability

The following information was supplied regarding data availability:

The data is available at GEO: GSE66676 and GSE130970. The PCR data are available in the Supplemental Files.

Supplemental Information

Supplemental information for this article can be found online at http://dx.doi.org/10.7717/peerj.17011#supplemental-information.

REFERENCES

Arab JP, Arrese M, Trauner M. 2018. Recent Insights into the Pathogenesis of Non-alcoholic Fatty Liver Disease. *Annual Review of Pathology: Mechanisms of Disease* **13**:321–350 DOI 10.1146/annurev-pathol-020117-043617.

Beheshti Namdar A, Ahadi M, Hoseini SM, Vosoghinia H, Rajablou H, Farsi S, Zangouei A, Rahimi HR. 2023. Effect of nano-micelle curcumin on hepatic enzymes: a new treatment approach for non-alcoholic fatty liver disease (NAFLD). *Avicenna Journal of Phytomedicine* **13**:615–625 DOI 10.22038/AJP.2023.21919.

Byrnes K, Blessinger S, Bailey NT, Scaife R, Liu G, Khambu B. 2022. Therapeutic regulation of autophagy in hepatic metabolism. *Acta Pharmaceutica Sinica B* **12**:33–49 DOI 10.1016/j.apsb.2021.07.021.

Cao Z, Guan L, Yu R, Chen J. 2022. Identifying autophagy-related lncRNAs and potential ceRNA networks in NAFLD. *Frontiers in Genetics* **13**:931928 DOI 10.3389/fgene.2022.931928.

Cao P, Yue M, Cheng Y, Sullivan MA, Chen W, Yu H, Li F, Wu S, Lv Y, Zhai X, Zhang Y. 2023. Naringenin prevents non-alcoholic steatohepatitis by modulating the host

metabolome and intestinal microbiome in MCD diet-fed mice. *Food Science & Nutrition* **11**:7826–7840 DOI 10.1002/fsn3.3700.

Chen F, Gong E, Ma J, Lin J, Wu C, Chen S, Hu S. 2022. Prognostic score model based on six m6A-related autophagy genes for predicting survival in esophageal squamous cell carcinoma. *Journal of Clinical Laboratory Analysis* **36**:e24507 DOI 10.1002/jcla.24507.

Chen X, Ishwaran H. 2012. Random forests for genomic data analysis. *Genomics* **99**:323–329 DOI 10.1016/j.ygeno.2012.04.003.

Chen SW, Yin GL, Song CY, Meng DC, Yu WF, Zhang X, Feng YN, Liang PP, Zhang FX. 2023. Diosgenin alleviates NAFLD induced by a high-fat diet in rats *via* mTOR/SREBP-1c/HSP60/MCAD/SCAD signaling pathway. *Zhongguo Zhong Yao Za Zhi* **48**:5304–5314.

Cheng X, Ma X, Zhu Q, Song D, Ding X, Li L, Jiang X, Wang X, Tian R, Su H, Shen Z, Chen S, Liu T, Gong W, Liu W, Sun Q. 2019. Pacer Is a Mediator of mTORC1 and GSK3-TIP60 Signaling in Regulation of Autophagosome Maturation and Lipid Metabolism. *Molecular Cell* **73**:788–802. e787 DOI 10.1016/j.molcel.2018.12.017.

Cheng J, Moyer BD, Milewski M, Loffing J, Ikeda M, Mickle JE, Cutting GR, Li M, Stanton BA, Guggino WB. 2002. A Golgi-associated PDZ domain protein modulates cystic fibrosis transmembrane regulator plasma membrane expression. *Journal of Biological Chemistry* **277**:3520–3529 DOI 10.1074/jbc.M110177200.

Coune PG, Bensadoun JC, Aebischer P, Schneider BL. 2011. Rab1A over-expression prevents Golgi apparatus fragmentation and partially corrects motor deficits in an alpha-synuclein based rat model of Parkinson's disease. *Journal of Parkinson's Disease* **1**:373–387 DOI 10.3233/JPD-2011-11058.

Di Malta C, Cinque L, Settembre C. 2019. Transcriptional Regulation of Autophagy: Mechanisms and Diseases. *Frontiers in Cell and Developmental Biology* **7**:114 DOI 10.3389/fcell.2019.00114.

Estes C, Razavi H, Loomba R, Younossi Z, Sanyal AJ. 2018. Modeling the epidemic of nonalcoholic fatty liver disease demonstrates an exponential increase in burden of disease. *Hepatology* **67**:123–133 DOI 10.1002/hep.29466.

Hazari Y, Pedro JMBravo-San, Hetz C, Galluzzi L, Kroemer G. 2020. Autophagy in hepatic adaptation to stress. *Journal of Hepatology* **72**:183–196 DOI 10.1016/j.jhep.2019.08.026.

He J, Bellini M, Xu J, Castleberry AM, Hall RA. 2004. Interaction with cystic fibrosis transmembrane conductance regulator-associated ligand (CAL) inhibits beta1-adrenergic receptor surface expression. *Journal of Biological Chemistry* **279**:50190–50196 DOI 10.1074/jbc.M404876200.

He L, Li H, Wu A, Peng Y, Shu G, Yin G. 2019. Functions of N6-methyladenosine and its role in cancer. *Molecular Cancer* **18**:176 DOI 10.1186/s12943-019-1109-9.

He Q, Zeng J, Yao K, Wang W, Wu Q, Tang R, Xia X, Zou X. 2020. Long-term subcutaneous injection of lipopolysaccharides and high-fat diet induced non-alcoholic fatty liver disease through IKKepsilon/NF-kappaB signaling. *Biochemical and Biophysical Research Communications* **532**:362–369 DOI 10.1016/j.bbrc.2020.08.036.

Henning JR, Graffeo CS, Rehman A, Fallon NC, Zambirinis CP, Ochi A, Barilla R, Jamal M, Deutsch M, Greco S, Ego-Osuala M, Bin-Saeed U, Rao RS, Badar S, Quesada JP, Acehan D, Miller G. 2013. Dendritic cells limit fibroinflammatory injury in nonalcoholic steatohepatitis in mice. *Hepatology* **58**:589–602 DOI 10.1002/hep.26267.

Hoang SA, Oseini A, Feaver RE, Cole BK, Asgharpour A, Vincent R, Siddiqui M, Lawson MJ, Day NC, Taylor JM, Wamhoff BR, Mirshahi F, Contos MJ, Idowu M, Sanyal AJ. 2019. Gene expression predicts histological severity and reveals distinct molecular profiles of nonalcoholic fatty liver disease. *Scientific Reports* **9**:12541 DOI 10.1038/s41598-019-48746-5.

Huang T, Chen B, Wang F, Cai W, Wang X, Huang B, Liu F, Jiang B, Zhang Y. 2021. Rab1A promotes IL-4R/JAK1/STAT6-dependent metastasis and determines JAK1 inhibitor sensitivity in non-small cell lung cancer. *Cancer Letters* **523**:182–194 DOI 10.1016/j.canlet.2021.10.008.

Huh JY, Reilly SM, Abu-Odeh M, Murphy AN, Mahata SK, Zhang J, Cho Y, Seo JB, Hung CW, Green CR, Metallo CM, Saltiel AR. 2020. TANK-binding kinase 1 regulates the localization of Acyl-CoA Synthetase ACSL1 to control hepatic fatty acid oxidation. *Cell Metabolism* **32**:1012–1027. e1017 DOI 10.1016/j.cmet.2020.10.010.

Kakino S, Ohki T, Nakayama H, Yuan X, Otabe S, Hashinaga T, Wada N, Kurita Y, Tanaka K, Hara K, Soejima E, Tajiri Y, Yamada K. 2018. Pivotal role of TNF-alpha in the development and progression of nonalcoholic fatty liver disease in a murine model. *Hormone and Metabolic Research* **50**:80–87 DOI 10.1055/s-0043-118666.

Kanwal F, Kramer JR, Mapakshi S, Natarajan Y, Chayanupatkul M, Richardson PA, Li L, Desiderio R, Thrift AP, Asch SM, Chu J, El-Serag HB. 2018. Risk of hepatocellular cancer in patients with non-alcoholic fatty liver disease. *Gastroenterology* **155**:1828–1837. e1822 DOI 10.1053/j.gastro.2018.08.024.

Kurniawan DW, Jajoriya AK, Dhawan G, Mishra D, Argemi J, Bataller R, Storm G, Mishra DP, Prakash J, Bansal R. 2018. Therapeutic inhibition of spleen tyrosine kinase in inflammatory macrophages using PLGA nanoparticles for the treatment of non-alcoholic steatohepatitis. *Journal of Controlled Release* **288**:227–238 DOI 10.1016/j.jconrel.2018.09.004.

Lazarus JV, Mark HE, Villota-Rivas M, Palayew A, Carrieri P, Colombo M, Ekstedt M, Esmat G, George J, Marchesini G, Novak K, Ocama P, Ratziu V, Razavi H, Romero-Gomez M, Silva M, Spearman CW, Tacke F, Tsochatzis EA, Yilmaz Y, Younossi ZM, Wong VW, Zelber-Sagi S, Cortez-Pinto H, Anstee QM. Collaborators Npr. 2022. The global NAFLD policy review and preparedness index: Are countries ready to address this silent public health challenge? *Journal of Hepatology* **76**:771–780 DOI 10.1016/j.jhep.2021.10.025.

Li Z, Song Y, Wang M, Shen R, Qin K, Zhang Y, Jiang T, Chi Y. 2022. m6A regulator-mediated RNA methylation modification patterns are involved in immune microenvironment regulation of coronary heart disease. *Frontiers in Cardiovascular Medicine* **9**:905737 DOI 10.3389/fcvm.2022.905737.

Li Y, Wang J, Huang C, Shen M, Zhan H, Xu K. 2020. RNA N6-methyladenosine: a promising molecular target in metabolic diseases. *Cell & Bioscience* **10**:19 DOI 10.1186/s13578-020-00385-4.

Liu Q, Gregory RI. 2019. RNAmod: an integrated system for the annotation of mRNA modifications. *Nucleic Acids Research* **47**:W548–W555 DOI 10.1093/nar/gkz479.

Liu N, Zhou KI, Parisien M, Dai Q, Diatchenko L, Pan T. 2017. N6-methyladenosine alters RNA structure to regulate binding of a low-complexity protein. *Nucleic Acids Res* **45**:6051–6063 DOI 10.1093/nar/gkx141.

Luo Z, Zhang Z, Tai L, Zhang L, Sun Z, Zhou L. 2019. Comprehensive analysis of differences of N(6)-methyladenosine RNA methylomes between high-fat-fed and normal mouse livers. *Epigenomics* **11**:1267–1282 DOI 10.2217/epi-2019-0009.

Oral EA, Reilly SM, Gomez AV, Meral R, Butz L, Ajluni N, Chenevert TL, Korytnaya E, Neidert AH, Hench R, Rus D, Horowitz JF, Poirier B, Zhao P, Lehmann K, Jain M, Yu R, Liddle C, Ahmadian M, Downes M, Evans RM, Saltiel AR. 2017. Inhibition of IKKvarepsilon and TBK1 improves glucose control in a subset of patients with type 2 diabetes. *Cell Metabolism* **26**:157–170. e157 DOI 10.1016/j.cmet.2017.06.006.

Paredes-Turrubiarte G, Gonzalez-Chavez A, Perez-Tamayo R, Salazar-Vazquez BY, Hernandez VS, Garibay-Nieto N, Fragoso JM, Escobedo G. 2016. Severity of non-alcoholic fatty liver disease is associated with high systemic levels of tumor necrosis factor alpha and low serum interleukin 10 in morbidly obese patients. *Clinical and Experimental Medicine* **16**:193–202 DOI 10.1007/s10238-015-0347-4.

Peng Z, Gong Y, Wang X, He W, Wu L, Zhang L, Xiong L, Huang Y, Su L, Shi P, Cao X, Liu R, Li Y, Xiao H. 2022. METTL3-m(6)A-Rubicon axis inhibits autophagy in nonalcoholic fatty liver disease. *Molecular Therapy* **30**:932–946 DOI 10.1016/j.ymthe.2021.09.016.

Powell EE, Wong VW, Rinella M. 2021. Non-alcoholic fatty liver disease. *Lancet* **397**:2212–2224 DOI 10.1016/S0140-6736(20)32511-3.

Qin Y, Li B, Arumugam S, Lu Q, Mankash SM, Li J, Sun B, Li J, Flavell RA, Li HB, Ouyang X. 2021. m(6)A mRNA methylation-directed myeloid cell activation controls progression of NAFLD and obesity. *Cell Reports* **37**:109968 DOI 10.1016/j.celrep.2021.109968.

Qu C, Zheng D, Li S, Liu Y, Lidofsky A, Holmes JA, Chen J, He L, Wei L, Liao Y, Yuan H, Jin Q, Lin Z, Hu Q, Jiang Y, Tu M, Chen X, Li W, Lin W, Fuchs BC, Chung RT, Hong J. 2018. Tyrosine kinase SYK is a potential therapeutic target for liver fibrosis. *Hepatology* **68**:1125–1139 DOI 10.1002/hep.29881.

Reilly SM, Chiang SH, Decker SJ, Chang L, Uhm M, Larsen MJ, Rubin JR, Mowers J, White NM, Hochberg I, Downes M, Yu RT, Liddle C, Evans RM, Oh D, Li P, Olefsky JM, Saltiel AR. 2013. An inhibitor of the protein kinases TBK1 and IKK-varepsilon improves obesity-related metabolic dysfunctions in mice. *Nature Medicine* **19**:313–321 DOI 10.1038/nm.3082.

Rong L, Zou J, Ran W, Qi X, Chen Y, Cui H, Guo J. 2022. Advancements in the treatment of non-alcoholic fatty liver disease (NAFLD). *Frontiers in Endocrinology* **13**:1087260 DOI 10.3389/fendo.2022.1087260.

Sanz H, Valim C, Vegas E, Oller JM, Reverter F. 2018. SVM-RFE: selection and visualization of the most relevant features through non-linear kernels. *BMC Bioinformatics* **19**:432 DOI 10.1186/s12859-018-2451-4.

Seok S, Fu T, Choi SE, Li Y, Zhu R, Kumar S, Sun X, Yoon G, Kang Y, Zhong W, Ma J, Kemper B, Kemper JK. 2014. Transcriptional regulation of autophagy by an FXR-CREB axis. *Nature* **516**:108–111 DOI 10.1038/nature13949.

Song GJ, Jeon H, Seo M, Jo M, Suk K. 2018. Interaction between optineurin and Rab1a regulates autophagosome formation in neuroblastoma cells. *Journal of Neuroscience Research* **96**:407–415 DOI 10.1002/jnr.24143.

Tang W, Zhou J, Yang W, Feng Y, Wu H, Mok MTS, Zhang L, Liang Z, Liu X, Xiong Z, Zeng X, Wang J, Lu J, Li J, Sun H, Tian X, Yeung PC, Hou Y, Lee HM, Lam CCH, Leung HHW, Chan AWH, To KF, Wong J, Lai PBS, Ng KKC, Wong SKH, Wong VWS, Kong APS, Sung JJY, Cheng ASL. 2022. Aberrant cholesterol metabolic signaling impairs antitumor immunosurveillance through natural killer T cell dysfunction in obese liver. *Cellular & Molecular Immunology* **19**:834–847 DOI 10.1038/s41423-022-00872-3.

Tremel S, Ohashi Y, Morado DR, Bertram J, Perisic O, Brandt LTL, Von Wrisberg MK, Chen ZA, Maslen SL, Kovtun O, Skehel M, Rappsilber J, Lang K, Munro S, Briggs JAG, Williams RL. 2021. Structural basis for VPS34 kinase activation by Rab1 and Rab5 on membranes. *Nature Communications* **12**:1564 DOI 10.1038/s41467-021-21695-2.

Ueno T, Komatsu M. 2017. Autophagy in the liver: functions in health and disease. *Nature Reviews Gastroenterology & Hepatology* **14**:170–184 DOI 10.1038/nrgastro.2016.185.

Wan J, Benkdane M, Teixeira-Clerc F, Bonnafous S, Louvet A, Lafdil F, Pecker F, Tran A, Gual P, Mallat A, Lotersztajn S, Pavoine C. 2014. M2 Kupffer cells promote M1 Kupffer cell apoptosis: a protective mechanism against alcoholic and nonalcoholic fatty liver disease. *Hepatology* **59**:130–142 DOI 10.1002/hep.26607.

Wang YY, Lin HL, Wang KL, Que GX, Cao T, Zhu LM, Yang X, Yang XF. 2023. Influence of gut microbiota and its metabolites on progression of metabolism-associated fatty liver disease. *Chinese Medical Sciences Journal* **38**:286–296 DOI 10.24920/004220.

Wang Y, Wang Z, Sun J, Qian Y. 2021. Identification of HCC Subtypes With Different Prognosis and Metabolic Patterns Based on Mitophagy. *Frontiers in Cell and Developmental Biology* **9**:799507 DOI 10.3389/fcell.2021.799507.

Wang X, Wu R, Liu Y, Zhao Y, Bi Z, Yao Y, Liu Q, Shi H, Wang F, Wang Y. 2020. m(6)A mRNA methylation controls autophagy and adipogenesis by targeting Atg5 and Atg7. *Autophagy* **16**:1221–1235 DOI 10.1080/15548627.2019.1659617.

Webster CP, Smith EF, Bauer CS, Moller A, Hautbergue GM, Ferraiuolo L, Myszczynska MA, Higginbottom A, Walsh MJ, Whitworth AJ, Kaspar BK, Meyer K, Shaw PJ, Grierson AJ, De Vos KJ. 2016. The C9orf72 protein interacts with Rab1a and the ULK1 complex to regulate initiation of autophagy. *The EMBO Journal* **35**:1656–1676 DOI 10.15252/embj.201694401.

Xanthakos SA, Jenkins TM, Kleiner DE, Boyce TW, Mourya R, Karns R, Brandt ML, Harmon CM, Helmrath MA, Michalsky MP, Courcoulas AP, Zeller MH, Inge TH, Teen LC. 2015. High Prevalence of Nonalcoholic Fatty Liver Disease in Adolescents Undergoing Bariatric Surgery. *Gastroenterology* **149**:623–634. e628 DOI 10.1053/j.gastro.2015.05.039.

Xie W, Ma LL, Xu YQ, Wang BH, Li SM. 2019. METTL3 inhibits hepatic insulin sensitivity *via* N6-methyladenosine modification of Fasn mRNA and promoting fatty acid metabolism. *Biochemical and Biophysical Research Communications* **518**:120–126 DOI 10.1016/j.bbrc.2019.08.018.

Xiong X, Tao R, DePinho RA, Dong XC. 2012. The autophagy-related gene 14 (Atg14) is regulated by forkhead box O transcription factors and circadian rhythms and plays a critical role in hepatic autophagy and lipid metabolism. *Journal of Biological Chemistry* **287**:39107–39114 DOI 10.1074/jbc.M112.412569.

Xu J, Jia YF, Tapadar S, Weaver JD, Raji IO, Pithadia DJ, Javeed N, Garcia AJ, Choi DS, Matveyenko AV, Oyelere AK, Shin CH. 2018. Inhibition of TBK1/IKKepsilon promotes regeneration of pancreatic beta-cells. *Scientific Reports* **8**:15587 DOI 10.1038/s41598-018-33875-0.

Xu S, Wang Y, Li Z, Hua Q, Jiang M, Fan X. 2022. LncRNA GAS5 knockdown mitigates hepatic lipid accumulation *via* regulating MiR-26a-5p/PDE4B to activate cAMP/CREB pathway. *Frontiers in Endocrinology* **13**:889858 DOI 10.3389/fendo.2022.889858.

Yang F, Jin H, Que B, Chao Y, Zhang H, Ying X, Zhou Z, Yuan Z, Su J, Wu B, Zhang W, Qi D, Chen D, Min W, Lin S, Ji W. 2019. Dynamic m(6)A mRNA methylation reveals the role of METTL3-m(6)A-CDCP1 signaling axis in chemical carcinogenesis. *Oncogene* **38**:4755–4772 DOI 10.1038/s41388-019-0755-0.

Yang XZ, Li XX, Zhang YJ, Rodriguez-Rodriguez L, Xiang MQ, Wang HY, Zheng XF. 2016. Rab1 in cell signaling, cancer and other diseases. *Oncogene* **35**:5699–5704 DOI 10.1038/onc.2016.81.

Yu G, Wang LG, Han Y, He QY. 2012. clusterProfiler: an R package for comparing biological themes among gene clusters. *OMICS* **16**:284–287 DOI 10.1089/omi.2011.0118.

Zacksenhaus E, Liu JC, Jiang Z, Yao Y, Xia L, Shrestha M, Ben-David Y. 2017. Transcription factors in breast cancer-lessons from recent genomic analyses and therapeutic implications. *Advances in Protein Chemistry and Structural Biology* **107**:223–273 DOI 10.1016/bs.apcsb.2016.10.003.

Zamanian MY, Sadeghi Ivraghi M, Khachatryan LG, Vadiyan DE, Bali HY, Golmohammadi M. 2023. A review of experimental and clinical studies on the therapeutic effects of pomegranate (Punica granatum) on non-alcoholic fatty liver disease: Focus on oxidative stress and inflammation. *Food Science & Nutrition* **11**:7485–7503 DOI 10.1002/fsn3.3713.

Zeng Q, Liu CH, Ampuero J, Wu D, Jiang W, Zhou L, Li H, Bai L, Romero-Gomez M, Tang H. 2024. Circular RNAs in non-alcoholic fatty liver disease: functions and clinical significance. *RNA Biology* **21**:1–15 DOI 10.1080/15476286.2023.2290769.

Zhai Q, Wu H, Zheng S, Zhong T, Du C, Yuan J, Peng J, Cai C, Li J. 2023. Association between gut microbiota and NAFLD/NASH: a bidirectional two-sample Mendelian randomization study. *Frontiers in Cellular and Infection Microbiology* **13**:1294826 DOI 10.3389/fcimb.2023.1294826.

Zhang MY, Huo C, Liu JY, Shi ZE, Zhang WD, Qu JJ, Yue YL, Qu YQ. 2021a. Identification of a Five Autophagy Subtype-Related Gene Expression Pattern for Improving the Prognosis of Lung Adenocarcinoma. *Frontiers in Cell and Developmental Biology* **9**:756911 DOI 10.3389/fcell.2021.756911.

Zhang Y, Najmi SM, Schneider DA. 2017. Transcription factors that influence RNA polymerases I and II: To what extent is mechanism of action conserved? *Biochimica et Biophysica Acta (BBA)—Gene Regulatory Mechanisms* **1860**:246–255 DOI 10.1016/j.bbagrm.2016.10.010.

Zhang X, Wang X, Yuan Z, Radford SJ, Liu C, Libutti SK, Zheng XFS. 2021b. Amino acids-Rab1A-mTORC1 signaling controls whole-body glucose homeostasis. *Cell Reports* **34**:108830 DOI 10.1016/j.celrep.2021.108830.

Zhao P, Wong KI, Sun X, Reilly SM, Uhm M, Liao Z, Skorobogatko Y, Saltiel AR. 2018. TBK1 at the crossroads of inflammation and energy homeostasis in adipose tissue. *Cell* **172**:731–743. e712 DOI 10.1016/j.cell.2018.01.007.

Zheng Y, Fang D, Huang C, Zhao L, Gan L, Chen Y, Liu F. 2021. Gentiana scabra restrains hepatic pro-inflammatory macrophages to ameliorate non-alcoholic fatty liver disease. *Frontiers in Pharmacology* **12**:816032 DOI 10.3389/fphar.2021.816032.

Zhou Z, Qi J, Lim CW, Kim JW, Kim B. 2020b. Dual TBK1/IKKepsilon inhibitor amlexanox mitigates palmitic acid-induced hepatotoxicity and lipoapoptosis *in vitro*. *Toxicology* **444**:152579 DOI 10.1016/j.tox.2020.152579.

Zhou J, Zhou F, Wang W, Zhang XJ, Ji YX, Zhang P, She ZG, Zhu L, Cai J, Li H. 2020a. Epidemiological Features of NAFLD From 1999 to 2018 in China. *Hepatology* **71**:1851–1864 DOI 10.1002/hep.31150.